Journal of Power Sources 196 (2011) 1205–1215

Contents lists available at ScienceDirect

Journal of Power Sources

journal homepage: www.elsevier.com/locate/jpowsour

# Fuel cell system modeling for solid oxide fuel cell/gas turbine hybrid power plants, Part I: Modeling and simulation framework

Florian Leucht[a,*], Wolfgang G. Bessler[a,b], Josef Kallo[a], K. Andreas Friedrich[a,b], H. Müller-Steinhagen[a,b]

[a] German Aerospace Centre (DLR), Institute of Technical Thermodynamics, Section of Electrochemical Energy Conversion, Pfaffenwaldring 38-40, 70569 Stuttgart, Germany
[b] University of Stuttgart, Institute of Thermodynamics and Thermal Engineering, Pfaffenwaldring 6, 70550 Stuttgart, Germany

ARTICLE INFO

*Article history:*
Received 30 March 2010
Received in revised form 11 August 2010
Accepted 25 August 2010

*Keywords:*
SOFC
System
Pressurized
Modeling
Dynamic

ABSTRACT

A sustainable future power supply requires high fuel-to-electricity conversion efficiencies even in small-scale power plants. A promising technology to reach this goal is a hybrid power plant in which a gas turbine (GT) is coupled with a solid oxide fuel cell (SOFC). This paper presents a dynamic model of a pressurized SOFC system consisting of the fuel cell stack with combustion zone and balance-of-plant components such as desulphurization, humidification, reformer, ejector and heat exchangers. The model includes thermal coupling between the different components. A number of control loops for fuel and air flows as well as power management are integrated in order to keep the system within the desired operation window. Models and controls are implemented in a MATLAB/SIMULINK environment. Different hybrid cycles proposed earlier are discussed and a preferred cycle is developed. Simulation results show the prospects of the developed modeling and control system.



## 1. Introduction

An increased demand for new power plants in Germany and the European Union is expected. One main reason for this is that power plants originally built in the 1960s and 1970s will now have to be replaced. A second reason is the expected worldwide rise in electrical power demand by 70% in the first two decades of this century according to an estimation of the International Energy Agency (IEA). The demand for new power plants is expected to reach 200 GW in Europe and 40 GW in Germany [1]. With the known resources, this demand can only be satisfied by using highly efficient power plant processes as well as renewable energies. Furthermore, the distribution of electricity will have to be improved. Here, a main strategy is to decentralize the electrical power production in order to keep the distances between producer and consumer small.

Fuel cells and fuel cell systems are able to deliver electrical energy at electrical efficiencies above 50%. Large-scale fuel cell generators, as for example demonstrated by Siemens, are highly interesting for future power supply. For stationary applications, solid oxide fuel cells (SOFCs) have particular advantages [2]. They offer higher overall efficiencies as the waste heat from the system can be used for heating or process steam generation. In addition, they can be operated on readily available fuels (natural gas, diesel, etc.) with no or little reforming before entering the cell [3].

Coupling the fuel cells with a gas turbine (GT) further increases the efficiency [4]. This has two reasons. First, the fuel cell is operated under pressurized conditions (typically around 3–5 bar), which leads to an increased power output (higher performance) of the fuel cells. Secondly, the waste heat from the fuel cell stack is directly used in the gas turbine to drive the turbine and generate additional electricity. The pressurized hybrid system can easily reach over 60% electrical efficiency while the installed power can range from some ten kilowatt to the multi-megawatt range. Siemens has demonstrated the technology in the PH220 project which was sponsored by Southern California Edison and was installed and operated at the University of California, Irvine, in 2000 [4]. Since then, groups worldwide have investigated the technology and worked on the details of hybrid cycles for different SOFC and gas turbine technology.

An important topic in hybrid power plant and pressurized fuel cell technology is the durability of the cells and the balance-of-plant components. System lifetimes of over 40,000 h are required for economic viability [5]. We have recently shown in a theoretical study that higher pressures influence the equilibrium and the electrochemistry of nickel oxidation as well as carbon deposition, both of which lead to degradation of the SOFC [6]. In addition to this also the lifetime of system components, for example, the pressure vessels and the piping, have to be taken into consideration, as the

*Abbreviations:* AIT, air inlet tube; CZ, combustion zone; FU, fuel utilization; GT, gas turbine; $H_2$EQ, hydrogen equivalent; MEA, membrane-electrode assembly (fuel cell functional layers); OCV, open-circuit voltage; POx, partial oxidation burner; SOFC, solid oxide fuel cell; STCR, steam-to-carbon ratio.

* Corresponding author. Tel.: +49 711 6862-532.
*E-mail address:* Florian.Leucht@dlr.de (F. Leucht).

0378-7753/$ – see front matter © 2010 Elsevier B.V. All rights reserved.
doi:10.1016/j.jpowsour.2010.08.081

**Nomenclature**

| | |
|---|---|
| $a$ | activity |
| $c_P$ | heat capacity [J kg$^{-1}$] |
| $d$ | thickness [m] |
| $d_P$ | particle diameter [m] |
| $E^\circ$ | cell potential [V] |
| $F$ | Faraday constant, 96,485 C mol$^{-1}$ |
| $\Delta G$ | Gibbs free energy [J (K$^{-1}$ mol$^{-1}$)] |
| $i$ | current density [A m$^{-2}$] |
| $I$ | current [A] |
| $k$ | pre-exponential factor [A m$^{-2}$] |
| $l$ | length [m] |
| $m$ | mass [kg] |
| $M$ | molar mass [kg mol$^{-1}$] |
| $\dot{n}$ | mole flow [mol s$^{-1}$] |
| $p_i$ | partial pressure of species $i$ [Pa] |
| $\Delta p$ | pressure difference [Pa] |
| $P$ | pressure [Pa] |
| $\dot{Q}$ | heat flux [W] |
| $\rho$ | specific resistance [Ω cm] |
| $R$ | universal gas constant, 8.314 J (K$^{-1}$ mol$^{-1}$) |
| $t$ | time [s] |
| $T$ | temperature [K] |
| $u$ | velocity [m s$^{-1}$] |
| $V$ | voltage [V] |
| $\dot{V}$ | volume flow [m$^3$ s$^{-1}$] |
| $x_i$ | molar ratio of species $i$ |
| $z$ | number of electrons exchanged in reaction |
| $\alpha$ | symmetry factor in Tafel equation |
| $\varepsilon$ | porosity |
| $\eta$ | viscosity in Ergun equation [Pa s] |
| $\eta_i$ | overpotential [V] |
| $\lambda$ | friction factor of gas in tube |
| $\rho$ | density [kg m$^{-3}$] |
| $\zeta$ | tube friction factor |

*Sub- and superscripts*

| | |
|---|---|
| act | activation (e.g., overpotential) |
| air | air side |
| anode | anode side |
| captured | captured hydrogen sulphide in Eq. (1) |
| cathode | cathode side |
| cell | fuel cell |
| combustion | combustion |
| conc | concentration (e.g., overpotential) |
| conduct | conduction |
| conv | convection |
| $H_2S$ | hydrogen sulphide |
| mat | solid material |
| Nernst | Nernst potential (OCV) |
| NG | natural gas |
| Ohm | ohmic (e.g., overpotential) |
| overpot | overpotential |
| Ox | oxidation gases |
| rad | radiation |
| reac | reaction |
| recirc | recirculation |
| Red | reduction gases |
| ref | reference point (bulk) |
| seg | segment |
| spices | of involved species |

high temperature and the pressure in the SOFC system will accelerate the ageing of welded seams as well as the material itself. Even rather simple system components can be a source of failure [7] and should be examined closely on the way to pressurized operation of SOFC. For atmospheric systems this has been done in detail by Wärtsilä Corporation [8].

In this paper, we present a modeling and simulation framework for investigating the SOFC subsystem of SOFC/GT hybrid power plant. A background on potential system configurations is given. Component models of the SOFC subsystem including the fuel cell and balance-of-plant are presented in detail. Control approaches are discussed. Exemplary results are shown for a load profile imposed on the system. The focus of this paper is the presentation of the modeling framework. Part II of this two-part paper series [9] presents simulation applications. Different operation strategies applied to the system are investigated in order to enable a load-following operation in 24 h load cycles of residential areas. Also included in Part II is an economic evaluation of the modeled system.

## 2. Background

### 2.1. Research activities

Since Siemens tested the pressurized hybrid at the University of California (NFCRC, Irvine/California) in 2000, a large interest in hybrid SOFC/GT technologies has been observed worldwide. Several research groups are investigating hybrid power plants, as summarized in the following: In Italy the group of Massardo, Costamagna, Magistri and Traverso at the University of Genoa published results on part-load dynamics, control strategies as well as cycle layout [10]. For the SOFC they modeled tubular cells as well as the Rolls Royce integrated planar concept. In Sweden a group at Lund University around Assadi, Torisson and Selimovic [11,12] developed models for hybrid systems based on planar SOFC technology with a focus on the turbo machinery. In the United States, Samuelson and Brouwer with their group at NFCRC used their experience in operating the pressurized hybrid to deduce novel operating strategies for the hybrid system based on the Siemens tubular technology [13–15]. In Japan the group around Kobayashi, Ando and Nishiura from Mitsubishi Heavy Industries are working on pressurized hybrid systems in the 200 kW class [16]. They have been operating a combined cycle system with 75 kW in 2006. At the Norwegian University of Science and Technology (NTNU) the group of Bolland, Stiller and Thorud developed an SOFC hybrid system model toolbox [17,18]. The SOFC is based on the Siemens tubular technology and the system is similar to the CHP100 system configuration. For the hybrid system they examined different cycle configurations with different GT and SOFC integration levels.

The German Aerospace Centre (DLR, Stuttgart/Germany) has been working on this topic since 2006 in a joint research project with the University of Stuttgart [19,20]. The goal of this project is to install a hybrid power plant and to develop the technology to a pre-industrial level. In the first phase the complete system is modeled for close examination and cycle assessment. In the second phase an indirect coupling of the components is realized, that is, the turbo machinery data is used as an input on experimental work on a pressurized SOFC test rig while the results from the SOFC are used in the GT experiments. In the future third phase a small-scale power plant will be built in order to examine the component behavior and to demonstrate the technology.

### 2.2. System configurations

A number of possible system configurations for coupling of SOFC and GT have been reported in the literature. A key difference

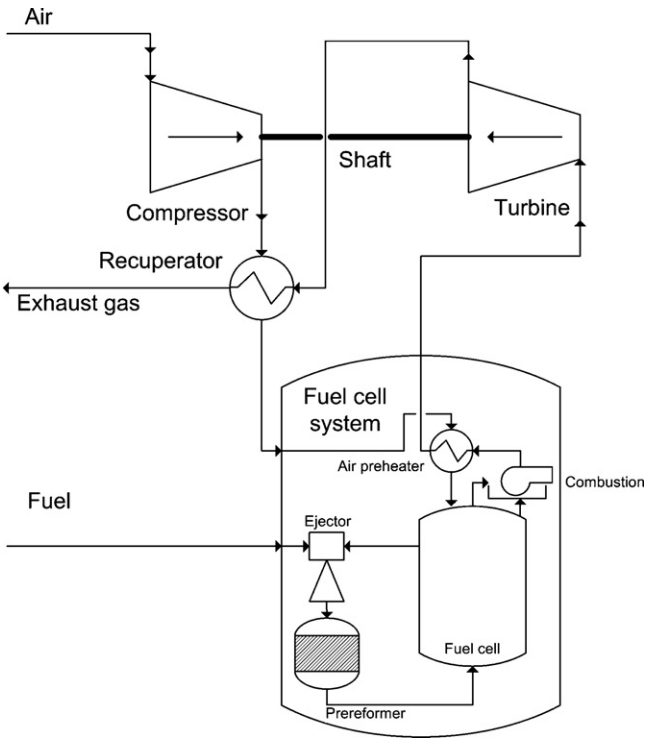


**Fig. 1.** Schematic of a simple pressurized hybrid cycle.

between the systems is the SOFC pressure. In this section different cycles are analyzed and the DLR preferred cycle is presented.

A simple cycle is shown in Fig. 1. Here the SOFC cathode is integrated between the compressor and the turbine while the fuel is compressed externally and fed to the SOFC system. The exhaust of the SOFC is then expanded into the turbine driving the compressor as well as the generator on the same shaft. This cycle has the advantage of a pressurized fuel cell while being very simple without any additional balance-of-plant components. Adding more heat exchangers might boost efficiency, but the system complexity increases and the interferences of the components leads to less stability. Panne et al. [20] performed steady-state calculations for this cycle and found a maximum electrical efficiency of approximately 49% at a rather low pressure ratio of the gas turbine of only 2.28. One key disadvantage of this system is that all fuel has to pass through the fuel cell. This may result in delays in turbine response time and high temperatures in the fuel cell combustion zone during load changes of the gas turbine.

Another possible cycle configuration is shown in Fig. 2. In this case the air is pressurized in the compressor, the recuperator transfers heat to the GT cycle and the air is expanded in the turbine. The SOFC system is located downstream of the turbine and is operated at pressures close to atmospheric pressure. As the recuperator has to deliver the desired turbine inlet temperature, additional fuel has to be injected into the system in order to maintain the operational limits of the GT. This configuration offers the possibility to operate the SOFC system at normal pressures while still having the additional benefit of the gas turbine cycle. The cycle design is quite simple although a ceramic recuperator would have to be used in the gas turbine system in order to reach the required temperature range of the GT system. However, these advantages have a detrimental effect on efficiency. Steady-state calculations have shown [20] that the maximum electrical efficiency of this system is below 39% for low pressure ratios and decreases further when going to higher pressure ratios. This can be explained by the additional fuel required in the combustor to meet the temperature demands.

From this comparison it becomes clear that the pressurized cycle arrangement should be preferred in order to reach high electrical efficiencies. In this cycle several modifications can be performed. Eliminating the combustion zone directly after the SOFC and passing the fuel cell off-gases to the GT combustor would result in a cleaner combustion and would enable the GT to produce the heat directly. However, the combustion zone serves as a plenum chamber, where large amounts of gas are stored. This enables the system to buffer short pressure deviations between anode and cathode. When eliminating the combustion zone, the pressure control of the system has to be very fast and able to maintain the two sides of the fuel cell at the same pressure. In order to allow the gas turbine to operate relatively independently from the SOFC system an additional combustor can be installed after the SOFC. This allows the GT to operate in stand-alone operation (i.e., without the SOFC supplying heat to the GT). Small load variations can be tackled by controlling the GT alone, reducing the influence on the SOFC operating conditions. For additional decoupling and an additional degree of freedom in the SOFC control, an air bypass can be introduced into the system. This allows air from the compressor to bypass the fuel cell thus cooling the fuel cell off-gas and maintaining pressure. If the SOFC would be out of operation for some reason, all air could be supplied to the GT directly. On the other hand, all air from the compressor can be delivered to the SOFC if, for example, the temperatures are too high. The SOFC off-gas is then supplied to the turbine.

A pressurized cycle with these modifications is shown in Fig. 3. It represents the preferred cycle studied at DLR. In this configuration the air is compressed by the GT compressor and preheated by the recuperator. A bypass valve divides the air stream into SOFC air and bypass air. Fuel is supplied separately and is treated in several stages before entering the fuel cell. A detailed schematic of the fuel cell subsystem is shown in Fig. 4. Natural gas is supplied to the system and desulphurized. Subsequently a humidifier is used to supply steam during low-load operation. Here, humidification can be achieved either by evaporating water or by a partial oxidation burner. After the part-load humidification the fuel enters an ejector

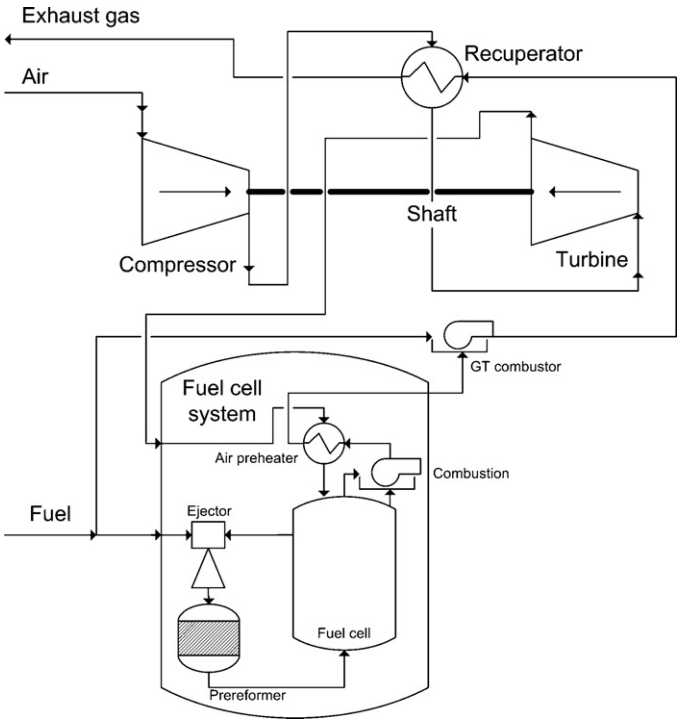


**Fig. 2.** Schematic of an atmospheric hybrid cycle.

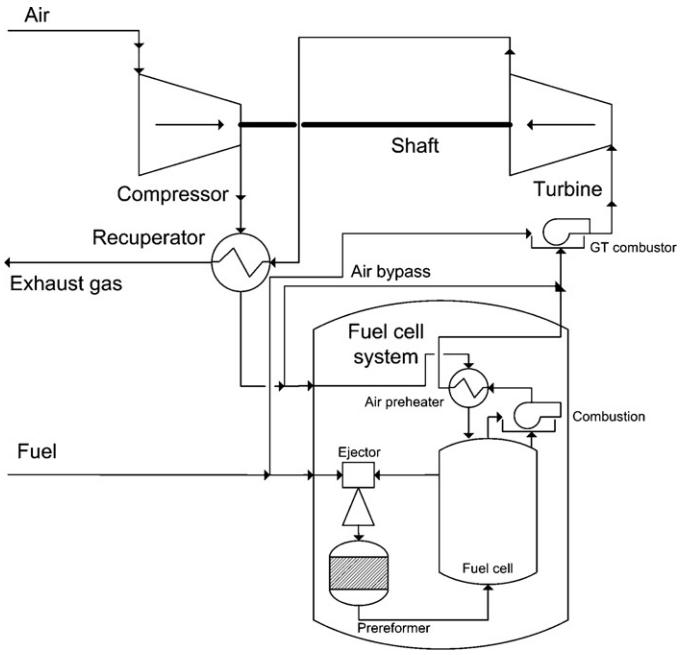


**Fig. 3.** Schematic of the preferred hybrid cycle.

for full-load humidification. The secondary stream (humid gas) to the ejector is supplied by the fuel cell anode off-gas just before the combustion zone. In this region the fuel is nearly depleted and is mainly composed of steam with low amounts of rest gases. The mixture exiting the ejector is fed to a steam pre-reformer converting the natural gas to a hydrogen-rich gas mixture. In a second reforming stage the gas is further converted inside the fuel cell stack. Finally the reformed fuel is supplied to the fuel cell anode. The depleted fuel which is not recirculated to the ejector is burned in the combustion zone and is utilized to preheat the air in a heat exchanger

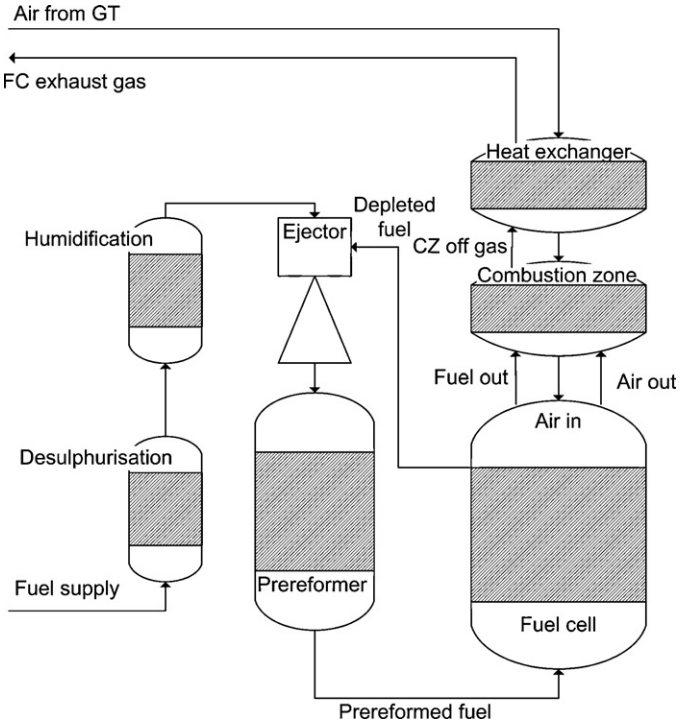


**Fig. 4.** Schematic of the SOFC subsystem of the preferred hybrid cycle shown in Fig. 3.

directly after the fuel cell. The preheated air is further heated in the combustion zone before entering the fuel cell stack in the so-called air inlet tubes of the tubular cells. At the closed end of the cells the direction of flow is reversed and the air enters the cathode side. Downstream of the cell the air is used to burn anode off-gas in the combustion zone as described above. The exhaust from the SOFC system is mixed with bypassed air and supplied to the GT combustor. If necessary, additional fuel is supplied to the combustor to keep the turbine inlet temperature at a desired value. The hot exhaust gas stream is expanded in the turbine and exits the hybrid system via the recuperator.

## 3. Modeling approach

### 3.1. Desulphurization

For power plants operating in a residential or industrial environment natural gas is the most likely fuel gas. However, sulphur compounds that are present in natural gas lead to anode poisoning and enhanced degradation due to surface site blocking and sulphide formation [21]. The main sulphur components in natural gas are hydrogen sulphide, which is a natural sulphur species, and mercaptanes, which are added as odoriser for safety reasons. Assuming the power plant will be situated at an unodorised natural gas pipeline the only sulphur species which has to be taken into account is hydrogen sulphide.

The desulphurisation is modeled in 0-D. The absorbent, zinc oxide, is integrated into the model as a fixed bed of pellets with the corresponding pressure loss and heat transfer correlations. The chemical reaction in the zinc oxide bed is described in Ref. [22]. The reactor performance is calculated from

$$m_{H_2S}^{captured} = M_{H_2S} \cdot \left( \frac{P \cdot \dot{V} \cdot x_{H_2S}}{RT} \right) \cdot t. \quad (1)$$

As can be seen from Eq. (1), the mass of hydrogen sulphide captured depends on pressure, temperature and volume flow. This is a straightforward approach for system modeling. Pressure losses are accounted for by the Ergun equation for pressure losses in fixed beds (cf. Eq. (8) below). The regeneration of the adsorbent, which is also described in Ref. [22], is not included in the model at the present stage. With regeneration the plant can be operated continuously without breaks for maintenance of the desulphurization unit.

### 3.2. Partial oxidation burner

In order to avoid large temperature gradients over the fuel cell, the natural gas used in the power plant should be reformed before entering the fuel cell. As the reformer utilized in this case is assumed to be a steam reformer, the supply of steam in adequate amounts has to be ensured. As described in Section 2.2, the steam supply in low-load operation is realized by partial oxidation (POx) of the fuel gas. In full-load operation it is realized via an ejector (see below).

The POx burner is modeled as a 0D model under the following assumptions: (1) The burner is a ceramic tube where a certain amount of air is injected, so that parts of the fuel gas are oxidized. (2) The combustible species present in the natural gas used as fuel ($CH_4$, $C_2H_6$, $H_2$, CO) react relative to their mole fraction to yield full oxidation products ($H_2O$, $CO_2$). (3) The complete oxygen is consumed; as oxygen is supplied in understoichiometric amounts, a corresponding fraction of fuel species leaves the burner unreacted. A similar approach was used to describe partial oxidation in a direct-flame fuel cell [23].

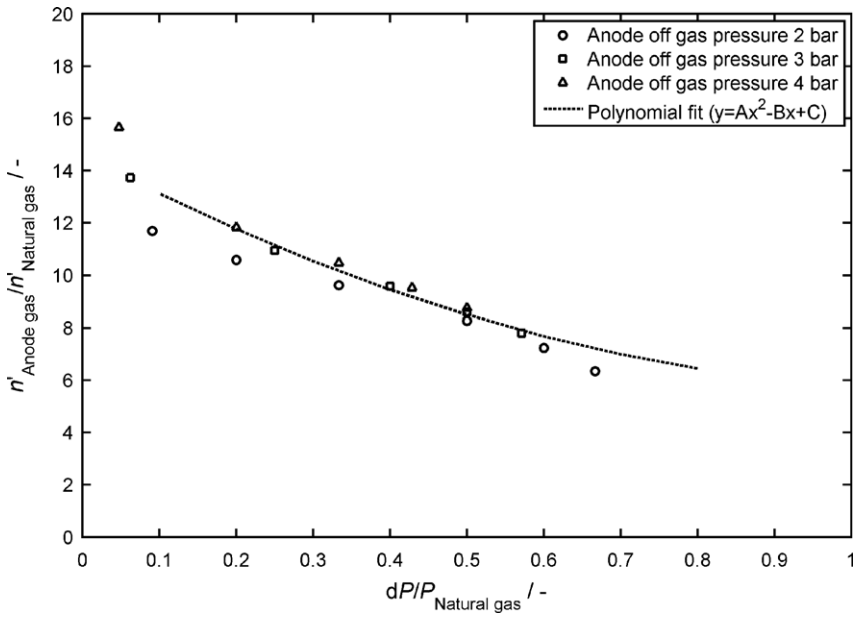


**Fig. 5.** Operating characteristics of ejector (molar flow ratio versus pressure difference over natural gas pressure) for anode off-gas pressures from 2 to 4 bar. Symbols show simulation results from a detailed ejector model, broken line shows polynomial fit used in simplified ejector model (Eq. (4)).

Pressure losses in the model are accounted for by the Bernoulli equation for pressure losses in tubes according to

$$\Delta p = \frac{\rho u^2}{2} \cdot \left(\lambda \cdot \frac{l}{d} + \zeta\right). \tag{2}$$

The heat balance for the model includes all heat sources and sinks,

$$T^{\mathrm{mat}} = \int \frac{\dot{Q}_{\mathrm{conv}} - \dot{Q}_{\mathrm{rad}} + \dot{Q}_{\mathrm{combustion}}}{m^{\mathrm{mat}} \cdot c_P^{\mathrm{mat}}} dt. \tag{3}$$

This equation includes the convective heat transfer from the material to the gas phase, the radiation heat transfer from the material to the POx burner casing as well as the heat of reaction from the combustion of the fuel gases.

In order to ensure the production of the proper amount of water needed in the reformer to reform hydrocarbons, a control loop is incorporated controlling the air stream to the POx burner (cf. Section 4.4).

### 3.3. Ejector

For full-load steam supply to the reformer an ejector is utilized. This ensures the steam supply to the system with only small penalties to the system efficiency. The ejector model is based on the ejector used by Stiller [17]. A detailed model was developed but showed too high computational cost to be used in the system simulation. A simpler model was therefore developed based on the data of the detailed ejector model. Fig. 5 shows the molar flow ratio between recirculated anode gas and fresh fuel for different anode gas pressures. Since the dependence on anode gas pressure is only moderate a polynomial fit shown according to

$$\dot{n}_{\mathrm{recirc,anode}} = \left(A \cdot \left(\frac{P_{\mathrm{NG}} - P_{\mathrm{anode}}}{P_{\mathrm{NG}}}\right)^2 + B \cdot \left(\frac{P_{\mathrm{NG}} - P_{\mathrm{anode}}}{P_{\mathrm{NG}}}\right) + C\right) \cdot \dot{n}_{\mathrm{NG}} \tag{4}$$

with $A = 6.82$, $B = -15.68$ and $C = 14.63$ is used for the calculation of the molar flow ratio in the simplified ejector model.

### 3.4. Reformer

The reformer ensures hydrogen supply to the fuel cell system. One could in principle also use natural gas directly, but this would result in large temperature gradients over the cell length and thus thermal stresses. The reformer is modeled as a cascade of ideal batch reactors filled with a fixed bed of reformer material. This represents a spatially discretized model along the flow path. The model is based on an equilibrium approach. Generally the reactions taking place in the reformer can be formulated as

$$\mathrm{C}_a\mathrm{H}_b + a \cdot \mathrm{H_2O} \rightleftharpoons \left(\frac{b}{2} + a\right) \mathrm{H_2} + a \cdot \mathrm{CO}. \tag{5}$$

Additionally, the water–gas shift reaction is included, where carbon monoxide is converted to hydrogen according to

$$\mathrm{CO} + \mathrm{H_2O} \rightleftharpoons \mathrm{CO_2} + \mathrm{H_2}. \tag{6}$$

The chemical equilibrium of these reactions can be expressed via

$$\prod x_i = \left(\frac{p^0}{p}\right)^{\sum \nu_i} \exp\left(-\frac{\Delta G}{RT}\right) \tag{7}$$

In addition to the equilibrium approach a simple temperature-dependent efficiency is incorporated in the model, where the efficiency drops if the temperature is below or above the ideal reformer temperature. Pressure losses are predicted by the Ergun equation for pressure losses in fixed bed reactors,

$$\Delta p = l \cdot (A\eta u_0 + B\rho u_0^2), \tag{8}$$

with

$$A = 150 \cdot \frac{(1-\varepsilon)^2}{\varepsilon^3 \cdot d_{\mathrm{P}}^2}, \quad B = 1.75 \cdot \frac{1-\varepsilon}{\varepsilon^3 \cdot d_{\mathrm{P}}}. \tag{9}$$

In the reformer model mass flow is determined by a pressure-backward approach. This means that the pressure from the downstream batch reactor is looped back to determine the mass flow from the upstream reactor. This can be directly developed from the ideal gas law,

$$p \cdot V = n \cdot R \cdot T. \tag{10}$$

For a pressure difference between two identical volumes at approximately the same temperature the relation between pres-

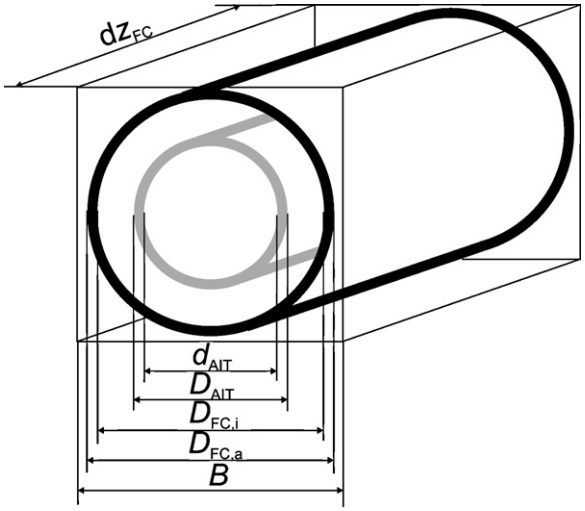


**Fig. 6.** Computational domain of a single fuel cell segment. The geometrical parameter values are given in Table 1.

sure difference and mole difference can be written as

$$\Delta n = \frac{\Delta p \cdot V}{R \cdot T}. \tag{11}$$

In this expression, $\Delta n$ is the number of moles, which has to flow from one reactor to the next in order to obtain the same pressure in both blocks. The resulting molar flow has to be integrated into the corresponding reactors' mole balances. When the pressure difference switches its sign, the mole flow reverses. In this case the composition from the downstream compartment is used to define the gas stream composition to the model block. The heat balance for each reactor is solved including the heat transferred between gas phase and solid material, the heat of reaction from the reforming reactions (5) and (6), the heat conduction from reactor to reactor, and the heat transferred by radiation to components close to the reformer; in case of the SOFC system this is the fuel cell stack.

### 3.5. Detailed fuel cell model

The fuel cell itself is the core of the fuel cell system. The fuel cell is modeled according to the tubular SOFC technology developed by Westinghouse and later advanced by Siemens Power Generation. The cell is based on a porous ceramic tube which is the cathode of the cell. Onto the cathode tube, electrolyte and anode layer are deposited via atmospheric plasma spraying technology. Fresh air is introduced into the tubular cell, which has a closed end at one side, through an air inlet tube (AIT). From a heat exchanger point of view, the tubular SOFC is a concentric tube heat exchanger, where cold air enters through the AIT, then turns around supplying oxygen to the cell reaction. On the outside of the cell, fuel gas is supplied in co-current flow. Fig. 6 shows a schematic representation of the cell. Table 1 lists the geometrical details of the compartments.

**Table 1**
Geometrical model parameters.

| Parameter (cf. Fig. 6) | Value | Unit |
|---|---|---|
| $dz_{FC}$ (detailed model) | 0.15 | m |
| $dz_{FC}$ (simplified model) | 0.5 | m |
| $d_{AIT}$ | 0.01 | m |
| $D_{AIT}$ | 0.012 | m |
| $D_{FC,i}$ | 0.01732 | m |
| $D_{FC,a}$ | 0.022 | m |
| $B_{kont}$ | 0.025 | m |

The detailed fuel cell model is based on a 1D + 1D approach. A 1D model of a cell segment represents the MEA, where transport processes are taking place through anode, electrolyte and cathode. Multiple segments are then coupled via gas-phase transport parallel to the MEA.

In SOFCs oxygen ions migrate through the electrolyte from the cathode to the anode and react with hydrogen, forming water at the anode side [2]. The half-cell reactions are given by

$$O_2 + 4e^- \rightleftharpoons 2O^{2-}(\text{cathode}) \tag{12}$$

$$2O^{2-} + 2H_2 \rightleftharpoons 2H_2O + 4e^-(\text{anode}) \tag{13}$$

In the current model, we use cell voltage as input parameter and calculate the cell (or segment) current using an iteration block included in Simulink. In order to calculate the cell voltage, the standard approach of subtracting overpotentials due to polarization losses from the open-circuit voltage (OCV or reversible cell voltage) is used [24],

$$V_{Cell} = V_{Nernst} - \eta_{act}^{anode} - \eta_{act}^{cathode} - \eta_{conc}^{anode} - \eta_{conc}^{cathode} - \eta_{Ohm} \tag{14}$$

The OCV is given by the Nernst equation,

$$V_{Nernst} = E^\circ + \frac{RT}{zF} \ln \frac{a_{Ox}}{a_{Red}}. \tag{15}$$

The anode activation overpotential is given by a Tafel equation

$$\eta_{act}^{anode} = \frac{RT}{(1-\alpha_{anode})zF} \cdot \ln \frac{i_{seg}}{i_{0,anode}} \tag{16}$$

The anode exchange current density $i_{0,a}$ is calculated via

$$i_{0,anode} = k_{anode} \frac{p_{H_2}}{p_{ref}} \cdot \left(\frac{p_{H_2O}}{p_{ref}}\right)^{0.5} \cdot \exp\left(-\frac{E_{act,anode}}{RT}\right). \tag{17}$$

For the cathode side the kinetics is given by

$$\eta_{act}^{cathode} = \frac{RT}{\alpha_{cathode} zF} \cdot \ln \frac{i_{seg}}{i_{0,cathode}} \tag{18}$$

$$i_{0,cathode} = k_{cathode} \frac{p_{O_2}}{p_{ref}} \cdot \exp\left(-\frac{E_{act,cathode}}{RT}\right). \tag{19}$$

In these equations, $E_{act}$ is the activation energy and $k$ the pre-exponential factor. The exchange current densities $i_0$ depend on reactant and product partial pressures described as (empirical) exponents. Various expressions for the anode exchange current density can be found in literature [17,25,26]; however, the formulations given above were found to fit the Siemens tubular system well. Note that Tafel kinetics are only strictly valid at sufficiently high overpotentials, while they violate thermodynamic consistency at open circuit ($i \neq 0$ for $\eta_{act} = 0$) [24]. For the current study, we use the computationally simple Tafel kinetics because we are only interested in polarized operating conditions.

Concentration overpotentials need to be included into the model in order to account for concentration profiles in the reactive layers. Because spatially resolved transport modeling [27] is computationally too expensive for system modeling, we use a simplified analytical expression for the concentration overpotentials according to

$$\eta_{conc}^{anode} = \frac{RT}{zF} \cdot \ln \frac{p_{species} + \gamma(T) \cdot i}{p_{species}} \tag{20}$$

$$\eta_{conc}^{cathode} = \frac{RT}{zF} \cdot \ln \frac{p_{O_2}}{p_{O_2} - \gamma(T) \cdot i} \tag{21}$$

for anode and cathode, respectively. Here, the drop in partial pressure of the reacting species through the porous electrodes is

**Table 2**
Electrochemical model parameters.

| Parameter | Value | Unit |
|---|---|---|
| $E_{act,anode}$ | 110 | kJ mol$^{-1}$ |
| $E_{act,cathode}$ | 110 | kJ mol$^{-1}$ |
| $k_{anode}$ | $7 \times 10^9$ | A m$^{-2}$ |
| $k_{cathode}$ | $7 \times 10^9$ | A m$^{-2}$ |
| $\rho_{anode}$ | 0.00033 | Ω cm |
| $\rho_{cathode}$ | 0.0125 | Ω cm |
| $\rho_{electrolyte}$ | 10 | Ω cm |
| $\rho_{interconnect}$ | 0.2 | Ω cm |

described by a empirical temperature-dependent factor $\gamma$ multiplied by the current density, where

$$\gamma = \frac{RT \cdot d_{anode}}{zF \cdot (0.021 \cdot (T/295)^{1.8})}. \quad (22)$$

The same expression can be used for the cathode side calculation.

Finally, the ohmic overpotential (23) is calculated from

$$\eta_{Ohm} = i_{seg} \cdot \sum_j \frac{\rho_j \cdot d_j}{A_{seg}}. \quad (23)$$

Here $i_{seg}$ is the current density in the considered cell segment, $\rho_j$ are the specific resistances of the layers of the cell, $d_j$ their thickness and $A_{seg}$ the cell segments reactive surface. Model parameters are given in Table 2.

Pressure losses are calculated according to Eq. (2) for the inner diameter of the AIT. In the gap between AIT and MEA the hydraulic diameter has to be used, which is calculated from

$$d = 4 \cdot \frac{f}{U}. \quad (24)$$

This formulation is also used for the volume between MEA and the computational boundary ($B$ in Table 1). The heat balance in the fuel cell has to be calculated for AIT and MEA material in parallel. The heat balance includes heat transfer between air and AIT; heat transfer between AIT and the cathode side gas mixture; heat transfer between the cell, the cathode side gas mixture and the anode side gas mixture; heat conduction to the neighboring model blocks from the AIT and from the cell; heat radiation from the cell to the AIT; heat radiation from the cell to the reformer; heat of formation of steam in the anode reactive layer; and heat production due to electrochemical losses (i.e., overpotentials). For the AIT temperature the heat balance is given by

$$T^{AIT} = \int \frac{\dot{Q}_{conv,air} + \dot{Q}_{conv,cathode} + \dot{Q}_{rad,AIT-MEA} + \dot{Q}_{conduct,AIT}}{m^{AIT} \cdot c_p^{AIT}} dt. \quad (25)$$

For the cell, the heat balance is given by

$$T^{MEA} = \int \frac{\dot{Q}_{conv,anode} + \dot{Q}_{conv,cathode} - \dot{Q}_{rad,AIT-MEA} + \dot{Q}_{reac} + \dot{Q}_{overpot} + \dot{Q}_{conduct,MEA} - \dot{Q}_{rad,MEA\text{-}REF}}{m^{MEA} \cdot c_p^{MEA}} dt \quad (26)$$

Simulated current–voltage characteristics from the fuel cell segment model are shown in Fig. 7. It can be seen from the figure that the voltage–current characteristics show the typical behavior, including parabolic shape at low currents and diffusion limitation at high currents.

From the segment model, the detailed fuel cell model is developed by repeating units of this segment. In the cell model it is assumed that the electrodes are on an equipotential surface. This is rather convenient as the cell voltage is the power-determining input to the cell model. The segments are interconnected for gas flow and heat conduction according to their position in the cell. The

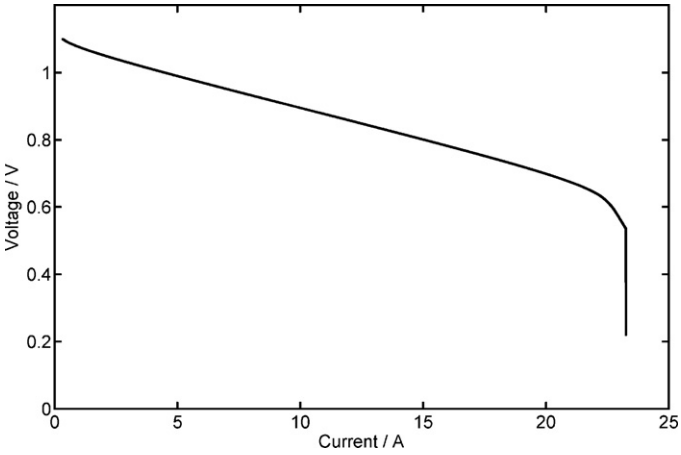


**Fig. 7.** Simulated voltage–current characteristics of a single fuel cell segment at 800 K cell temperature, 1.1 bar, 45% $H_2$, 9% CO, 7.5% $CO_2$, 38.5% $H_2O$.

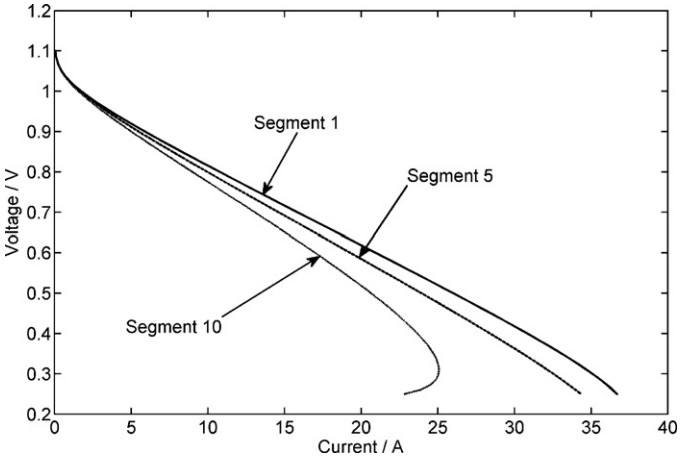


**Fig. 8.** Simulated voltage–current characteristics for segments 1, 5 and 10 of a 10-segment cell at 45% $H_2$, 9% CO, 7.5% $CO_2$, 38.5% $H_2O$, 1200 K cell temperature, 1.1 bar and a high fuel utilization of 97%.

detailed fuel cell model can be used to investigate the behavior of a cell in the stack under critical operation conditions. Exemplary simulation results are shown in Fig. 8. Here, the cell was discretized into 10 segments. While the voltage–current characteristics of the first segments of the cell do not show any signs of starvation within the investigated voltage window (down to 0.25 V), the current delivered by the last segment cannot be maintained at the previous level, as the upstream segments already convert a large part of the fuel. This results in a decrease in current from the last segment.

### 3.6. Simplified fuel cell model

The detailed fuel cell model discussed above was observed to be computationally too expensive to be used in system-level simulations. Especially during load changes, the model was not able to yield real-time simulations. We therefore chose to replace the detailed model by a look-up table. In order to maintain model accuracy over a large number of operating conditions, six dimensions were chosen for the table. The inputs are cell voltage, cell temper-

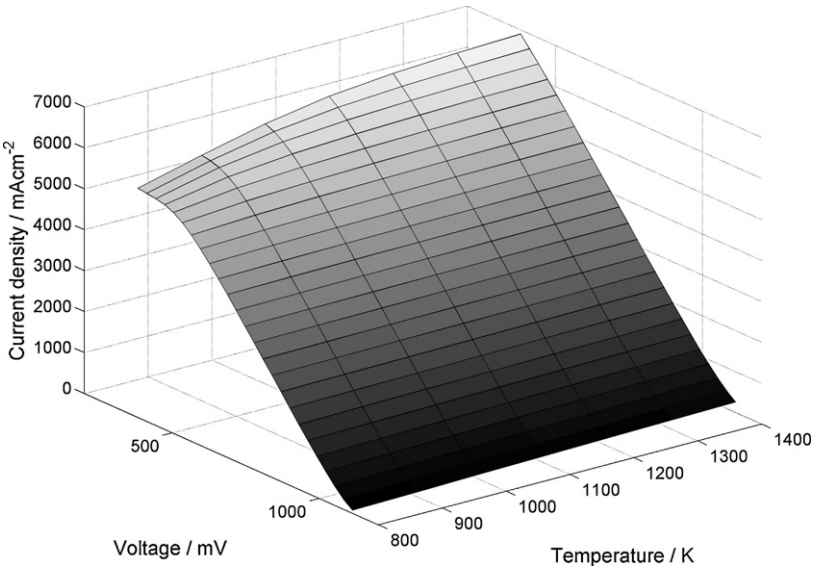


**Fig. 9.** Three-dimensional sub-set of the look-up table data for cell voltages from 1.2–0.4 V and temperatures from 800 to 1400 K at 1.1 bar, $H_2$:$H_2O$ = 70:30, with no inert species. Lines represent constant current in 500 mA $cm^{-2}$ steps.

ature, pressure, $H_2/H_2O$ ratio, and $H_2$/inert gas ratio. The output is the cell current as calculated from the detailed model. An example of a three-dimensional subset of the look-up table is shown in Fig. 9. Based on the detailed model, a matrix of $100 \times 7 \times 9 \times 5 \times 4$ values was calculated, which is linearly interpolated upon evaluation.

Heat balances and pressure losses are calculated as in the detailed models. In order to further decrease calculation time, the discretization was reduced from 10 segments to 3 segments. This was found to be sufficient to enable the model to show starvation influences. Overall, the simple fuel cell model is approximately ten times faster than the detailed fuel cell model.

In the system model, the anode off-gas is fed to the ejector model, where the recirculation rate is determined based on the pressure differences as explained above. The fraction of the off-gas not being recirculated is then fed to the combustion zone model.

### 3.7. Combustion zone model

During normal operating conditions, the fuel utilization of an SOFC will always be below 100%. This implies that the anode off-gas still contains non-oxidized gases. In the Siemens stack configuration the anode off-gas is fed to a combustion zone (CZ), where it is fully oxidized with the cathode off-gas, which is basically air with reduced oxygen content. The combustion relies on the fact that above a certain temperature hydrogen auto-ignites in the presence of oxygen. The CZ is not only utilized as a preheater for the air entering the fuel cell, but also as a pressure plenum chamber to buffer small pressure deviations between cathode and anode side.

In the model it is assumed that all combustible species in the off-gas are converted to $CO_2$ and $H_2O$. The corresponding heat of reaction is coupled into the heat balance of the model. Furthermore the CZ is assumed to exchange heat with the AIT of the fuel cell by means of heat conduction. The CZ temperature is a key control value of the system, as it shows the highest temperatures in normal operation. For CZ temperatures above ca. 1400 K the material of the AIT and the MEA will be destroyed, ending in the destruction of the fuel cell.

Directly downstream of the CZ a heat exchanger is included into the model enabling the system to exchange heat from the hot off-gases to the relatively cold air entering the AIT. The heat exchanger is discretized to achieve the characteristics of a tubular counter-flow heat exchanger. While one element represents the combustion zone itself, three additional elements represent the heat exchanger.

### 3.8. Coupling of components

The different component models described above are combined to a complete fuel cell system model as shown in Fig. 4. To reach this goal, a number of additional links are included. This includes thermal coupling of different components that allow heat transfer from the hotter parts of the system to the colder parts. In the tubular SOFC setup, the AIT runs through both the combustion zone and the fuel cell itself and is therefore thermally coupled via conductive heat transfer to both components. Heat exchange between fuel cell and reformer is modeled via radiation.

Note that the model has a number of so-called algebraic loops where data calculated downstream is relevant for upstream calculations. For example, depleted fuel leaving the cell is looped back via the ejector model, thus influencing the composition of the fresh fuel gas entering the generator. These loops result in additional computational effort.

## 4. Control approaches

### 4.1. Air flow management

As stated in the CZ model description, air flow management is one key control loop to be applied to the fuel cell. The air flow is controlled via a bypass valve (cf. Fig. 3). A valve position of zero means that all air from the compressor is bypassing the fuel cell, while a valve position of one corresponds to all air entering the fuel cell.

Two main reasons can be identified for the CZ temperature not being in the desired range of operation. Firstly, the fuel cell is still in start-up phase or not delivering much power. This would result in a rather low CZ temperature as no or little fuel is injected into the cycle. Secondly, if too much fuel is injected into the system or if the system is subject to a load decrease, the CZ temperature will be too high. In the second case, the remaining fuel in the fuel cell will not be used electrochemically but will be transported into the CZ, resulting in a strong temperature rise.

The control loop is programmed as a cascade of trigger temperatures. Depending on the CZ temperature the valve position is

set. In the normal operation range of the fuel cell system the valve positions are changed in rather small steps, mainly increasing the oxygen availability in the system. If the temperature exceeds the desired range of operation, for example because of a sudden load drop, the air mass flow to the fuel cell is raised up to 70% of the total air mass flow from the compressor.

### 4.2. Fuel flow management

Fuel flow management is crucial for save operation of a fuel cell system. Two main targets have to be achieved: The system has to be able to operate safely and the fuel utilization should be high to achieve high system efficiencies. In a real system there are non-ideal situations, for example fuel maldistribution (fuel not flowing through the cell but outside of the anode compartment thus not reacting). This leads to a fuel consumption of the system higher than the calculated fuel utilization. Therefore the fuel utilization is controlled to a value of 85%.

In general the fuel required to allow the system to deliver a certain current can be calculated as follows. Faraday's law allows calculating the molar flow of hydrogen required at a certain current,

$$\dot{n}_{H_2}^{\text{Faraday}} = \frac{I}{z \cdot F}. \tag{27}$$

As the fuel for the system is not pure hydrogen, a hydrogen equivalent,

$$H_2EQ = 4 \cdot \dot{n}_{CH_4} + 7 \cdot \dot{n}_{C_2H_6} + \dot{n}_{CO} + \dot{n}_{H_2}, \tag{28}$$

can be defined according to the oxidation reactions of the species in the fuel mass flow. Using the hydrogen equivalent, fuel molar flow to the system can be calculated according to

$$\dot{n}_{NG}^{\text{required}} = \frac{1}{FU} \cdot \frac{\dot{n}_{H_2}^{\text{Faraday}}}{H_2EQ}. \tag{29}$$

If a POx burner is used to assist steam supply to the system, the required fuel flow has to be increased by the fuel consumption of the burner itself,

$$\dot{n}_{NG}^{\text{add,POx}} = \dot{n}_{Air}^{\text{POx}} \cdot H_2EQ \cdot x_{O_2}. \tag{30}$$

which depends on POx air molar flow. Finally the required fuel molar flow can be calculated from

$$\dot{n}_{NG}^{\text{total}} = \dot{n}_{NG}^{\text{required}} + \dot{n}_{NG}^{\text{add,POx}}. \tag{31}$$

The difference between the system's delivered molar flow and the one required according to

$$e = \dot{n}_{NG}^{\text{total}} - \dot{n}_{NG}^{\text{system}}, \tag{32}$$

is utilized as the error $e$ in a PID controller controlling the fuel mass flow to the system.

During low-load operation the fuel injected into the system is set to higher values than actually needed. This helps the system starting operation from OCV, as otherwise the fuel present in the fuel cell would not be sufficient to support any load changes. This is done by setting a lower saturation boundary for the system current in the fuel control.

### 4.3. Power management

As described in Section 3.5, the voltage is used to define the operating point of the fuel cell. When controlling the voltage of a solid oxide fuel cell, it is important to keep the voltage above the electrochemical nickel oxidation voltage in order to avoid irreversible anode degradation. A temperature- and pressure-dependent expression for the nickel oxidation voltage $V_{NiOx}$ can be obtained from Ref. [28],

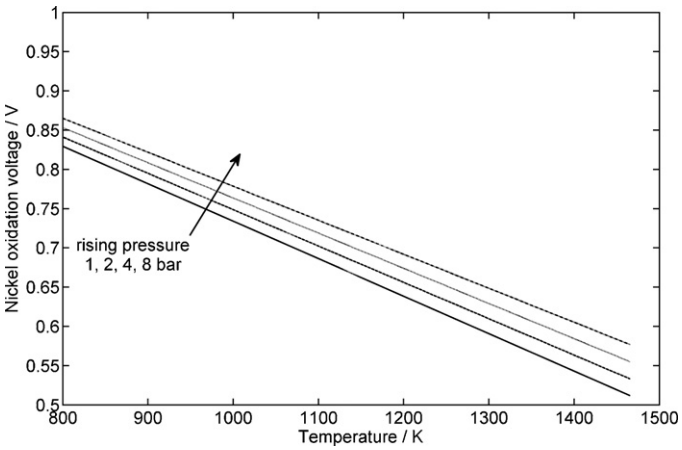


**Fig. 10.** Nickel oxidation voltage as a function of temperature at 1, 2, 4 and 8 bar according to Eq. (33).

$$V_{NiOx} = -\frac{RT}{zF} \cdot \ln\left(\frac{\sqrt{p_{O_2,Air}}}{\sqrt{p_{O_2,Ni-NiO}}}\right). \tag{33}$$

The equation gives the nickel oxidation voltage as a function of the oxygen partial pressure in air and the partial pressure of the oxygen enabling the nickel–nickel oxide transition. Fig. 10 shows a plot of $V_{NiOx}$ versus temperature. Nickel oxidation voltage drops linearly with increasing temperature. This means that the cell voltage can be lower at higher temperatures without destroying the anode. From Eq. (33) it can also be seen that the nickel oxidation is a function of oxygen partial pressure on the cathode side. This dependence is also shown in Fig. 10. It is important to realize that the cell voltage has to be higher under high-pressure operation in order to avoid cell degradation, a point of particular importance in the context of pressurized hybrid power plants.

In order to control the cell voltage, a voltage set point according to

$$V_{\text{Cell Demand}} = (1-f) \cdot V_{OCV} + f(\Delta V_{\text{safety}} + V_{NiOx}) \tag{34}$$

is used. In this expression, $f$ is a parameter determining the system voltage from OCV (0% load, $f = 0$) to full load (100% load, $f = 1$). As the system has to deal with non-idealities, a safety margin $\Delta V_{\text{safety}}$ is included in the equation, keeping the cell voltage sufficiently above the nickel oxidation voltage. This control does not interfere with the fuel control loop as the input for the fuel control is the outcome of the power control.

### 4.4. POx air control

In order to ensure a sufficiently high water production in the POx burner, a control loop was designed controlling the amount of air injected into the POx. The amount of water needed can be calculated via

$$\text{STCR} = \frac{\dot{n}_{H_2O}}{(\dot{n}_{CH_4} + 2 \cdot \dot{n}_{C_2H_6} + \dot{n}_{CO})} \tag{35}$$

and is normally used as a system analysis parameter called the steam-to-carbon ratio (STCR). For natural gas the desired STCR is in the range of 2.0–2.2 as the main component is methane requiring two moles of steam for each mole of methane for a full reformation to hydrogen. As high-quality natural gas consists of approximately 85–95% methane, the STCR can be approximated by

$$\text{STCR} = \frac{\dot{n}_{H_2O}}{\dot{n}_{NG}}. \tag{36}$$

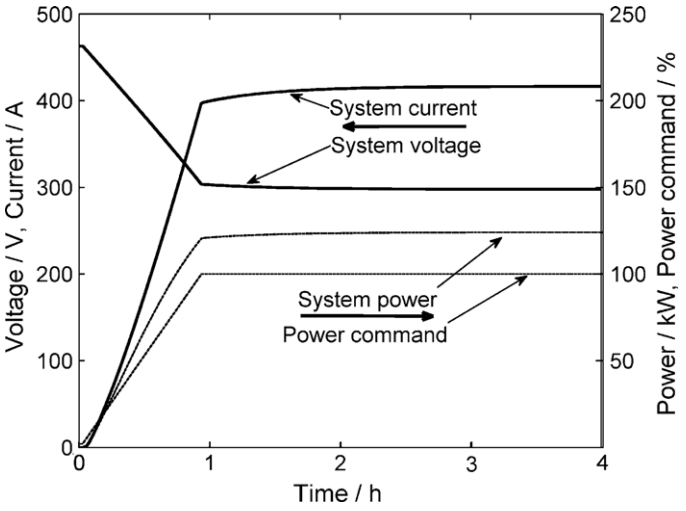


**Fig. 11.** Fuel cell system simulations: Load variation from OCV to 100% load at 4 bar system pressure and 1000 K temperature. Fuel is reformed natural gas. Power command on the right hand side axis is the power setpoint f in Eq. (34).

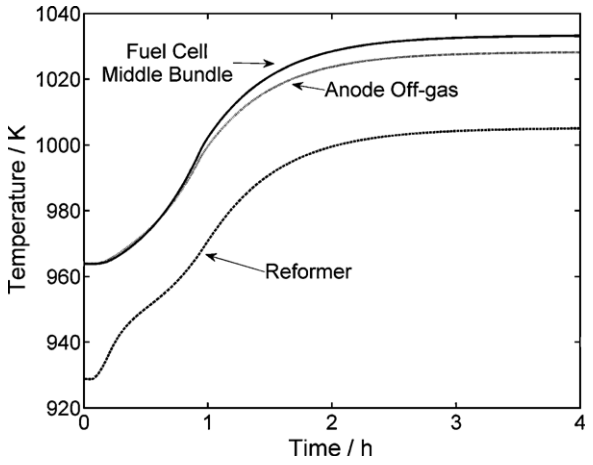


**Fig. 12.** Temperature transients during the load variation shown in Fig. 11.

From this expression, the required air molar flow to the POx reactor can be developed to

$$\dot{n}_{\mathrm{Air}} = \frac{1}{x_{\mathrm{O_2}}} \cdot \dot{n}_{\mathrm{O_2}} = \frac{1}{2 \cdot x_{\mathrm{O_2}}} \cdot \dot{n}_{\mathrm{H_2O}} = \frac{1}{2 \cdot x_{\mathrm{O_2}}} \cdot \mathrm{STCR} \cdot \dot{n}_{\mathrm{NG}}. \tag{37}$$

The amount of oxygen injected into the POx burner is controlled based on system current. As noted above, the burner is only used during start-up and low-load operation. Starting from a certain current the system is able to produce sufficient water to maintain the reforming process. With this the molar flow of air to the POx burner can be calculated from

$$\dot{n}_{\mathrm{Air}} = \left( \frac{I_{\mathrm{FC}}^{\mathrm{Max}}}{I_{\mathrm{FC}}^{\mathrm{actual}}} - 1 \right) \cdot \frac{5}{2} \cdot \mathrm{STCR} \cdot \dot{n}_{\mathrm{NG}}. \tag{38}$$

This expression may lead to negative air mass flow if the fuel cell current is higher than the set point; this is excluded using a saturation expression within Simulink.

## 5. Results

In this Section exemplary simulation results from the fuel cell system model are presented. A more detailed analysis, will be presented in part II of this publication [9].

For a system test run the dynamic load variation shown in Fig. 11 was applied to a 100 kW (atm) system model. The diagram shows the voltage and current response of the system when the load demand in the control loop is varied from 0 to 100% (right hand axis). For clarity, also the absolute power output of the system is depicted. Here, cell voltage is decreased linearly from 463 V (OCV) to 303.5 V (full load) during approximately one hour. It can be observed that the system voltage further decreases after the 3000 s ramp. This is due to the power control described above, as with rising system temperature the point of 100% load is moving to lower voltages. Power increases accordingly to 121 kW. The 21 kW gain on the nominal 100 kW system is a benefit of the increased system pressure (4 bar). As a result of the current drawn, the temperatures throughout the system rise (Fig. 12). The increase in temperature is delayed by approximately 200 s relative to the load change. It takes around 2 h after the load change for the temperature to stabilize at a new steady-state value. The response of the air flow management is shown in Fig. 13 which is a consequence of the control strategy of the system. The temperature increase triggers an increase in air flow in order to cool down the system and keep the CZ within the desired operating conditions. Because of the cascaded control architecture the mass flow increase with temperature rise is stepwise. Again, temperature control is delayed some hundred seconds relative to the load increase. When the first step in air flow is applied during the load change, a bend can be clearly seen in the system temperatures. The fuel flow control dynamics is shown in Fig. 14. During the whole simulated ramp, the fuel flow management keeps the deviation between needed and delivered fuel to relatively low values. Only at the beginning of the ramp, when the saturation described above is overcome, the deviation is close to 5%, but the system recovers within less than 10 min to normal values. Observe that the time line is stretched in the beginning to show the first minutes of the load change in more detail. The fuel utilization (FU) is shown in Fig. 15. During the large deviation between fuel mass flows (Fig. 14) the FU hits 100%, however only for a short time. This is not a major problem as the FU settles just below 100% thus still enabling the cell to operate safely.

The simulation shown here was performed on one CPU of an Intel® quad core 2.66 GHz desktop PC with 3 GB RAM. The computational time was one hour, while the simulated time is 3 h. Thus, real-time simulation could be achieved.

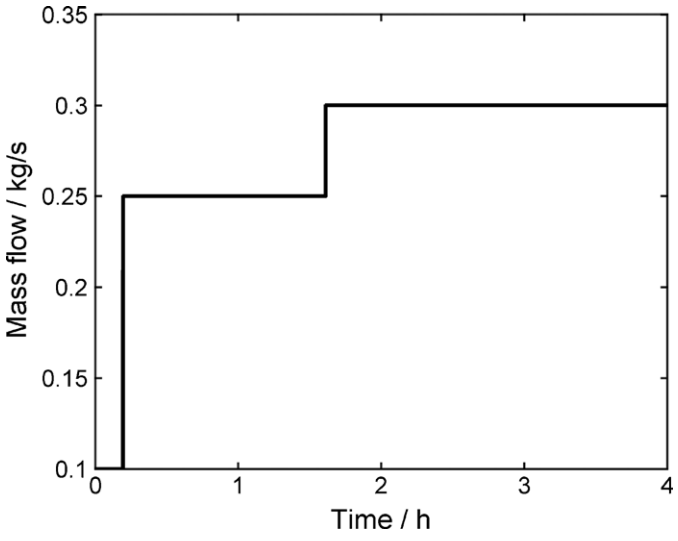


**Fig. 13.** Air flow dynamics as a result of temperature rise during the load variation shown in Fig. 11.

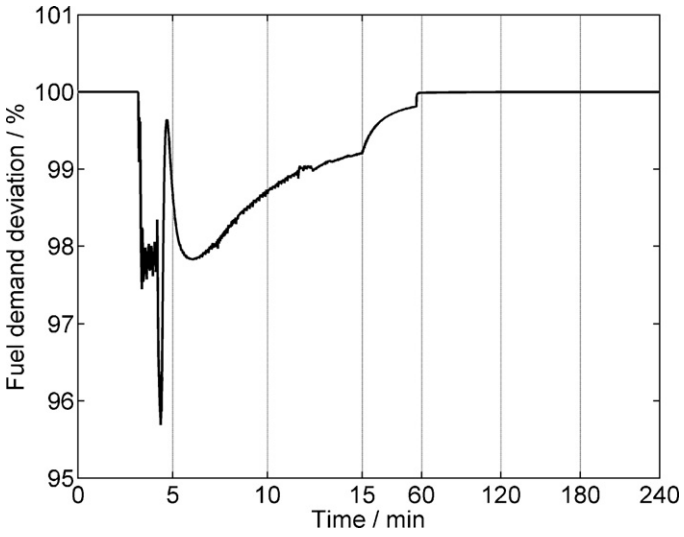


**Fig. 14.** Fuel flow control dynamics during the load variation shown in Fig. 11. The graph shows delivered fuel mass flow divided by demanded fuel mass flow. Observe that the time axis is stretched between 0 and 15 min.

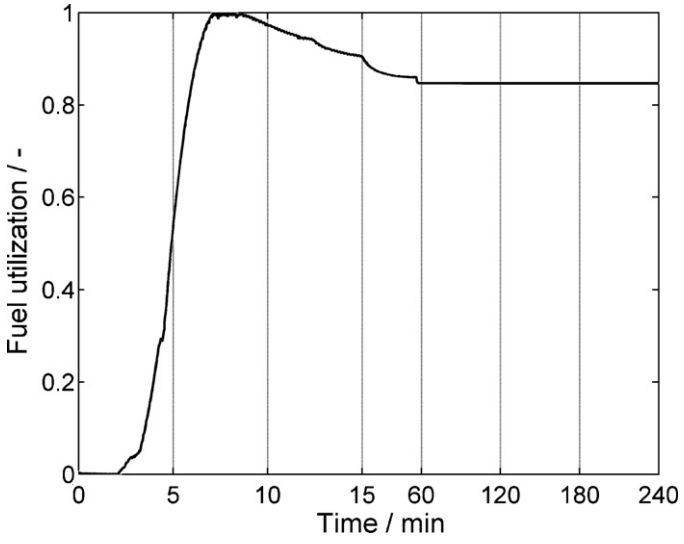


**Fig. 15.** Fuel utilization over time during the load variation shown in Fig. 11. Observe that also here the time axis is stretched between 0 and 15 min.

## 6. Conclusions

The development of an SOFC system model for application in GT/SOFC hybrid power plants was presented. Advantages and disadvantages of several hybrid cycle configurations proposed before were discussed. Based on this discussion, a preferred cycle arrangement for the SOFC generator in the hybrid system was developed.

The fuel cell subsystem of the preferred cycle was dynamically modeled in a MATLAB/SIMULINK environment. System components were implemented on different scales ranging from 0D models for smaller components (e.g., desulphurization), 1D models implemented as cascades of batch reactors for the reformer model, and 1D + 1D models for the tubular fuel cell and the combustion zone that include thermal and chemical interaction perpendicular to the flow direction. Several control loops designed to keep the fuel cell system in the desired range of operation were introduced.

It was demonstrated that the model is able to predict the dynamic operation of the SOFC system. Control loops are able to keep the system within a stable and safe operation range (temperature, fuel flow, air flow) avoiding conditions critical with respect to cell degradation. Detailed dynamic system simulations and system architecture analyses for the tubular SOFC system will be presented in the second part of this publication [9].

## Acknowledgements

This project is funded by the Helmholtz Association and the German Aerospace Centre (DLR). The collaboration with Prof. M. Aigner (DLR Institute of Combustion Technologies) and Prof. S. Staudacher (University of Stuttgart, Institute of Aircraft Propulsion Systems) is highly appreciated.

## References

[1] Cooretec, Forschungs- und Entwicklungskonzept für emisionsarme fossil befeuerte Kraftwerke, BWA, 2003.
[2] S.C. Singhal, K. Kendall, High-temperature Solid Oxide Fuel Cells: Fundamentals, Design and Applications, Elsevier Science, Oxford, 2003.
[3] B.C.H. Steele, Nature 400 (1999) 619–620.
[4] S.E. Veyo, L.A. Shockling, J.T. Dederer, J.E. Gillett, W.L. Lundberg, ASME Journal of Engineering for Gas Turbines and Power 124 (2002) 845–849.
[5] Fuel Cell Handbook (Seventh Edition), EG&G Technical Services, Inc., U.S. Department of Energy, Office of Fossil Energy, Natioal Energy Technology Laboratory, Morgantown, West Virginia, USA, 2004.
[6] M. Henke, J. Kallo, W.G. Bessler, Fuel Cells, submitted for publication.
[7] M. Halinen, J. Saarinen, M. Noponen, I.C. Vinke, J. Kiviaho, Fuel Cells 10 (2010) 440–462.
[8] K. Åström, E. Fontell, S. Virtanen, Journal of Power Sources 171 (2007) 46–54.
[9] F. Leucht, W.G. Bessler, J. Kallo, K.A. Friedrich, H. Müller-Steinhagen, Fuel Cell System Modeling for SOFC/GT Hybrid Power Plants, Part II: Dynamic Operation and Economic Analysis, in preparation.
[10] P. Costamagna, L. Magistri, A.F. Massardo, Journal of Power Sources 96 (2001) 352–368.
[11] M. Assadi, A. Hildebrandt, M. Kemm, F. Hermann, S. Ernebrant, CIMAC Congress 2004, 2004.
[12] A. Selimovic, Modelling of Solid Oxide Fuel Cells Applied to the Analysis of Integrated Systems with Gas Turbines, PhD Thesis, Lund University, 2002.
[13] F. Mueller, R. Gaynor, A.E. Auld, J. Brouwer, F. Jabbari, G.S. Samuelsen, Journal of Power Sources 176 (2008) 229–239.
[14] R. Roberts, J. Brouwer, F. Jabbari, T. Junker, H. Ghezel-Ayagh, Journal of Power Sources 161 (2006) 484–491.
[15] Y. Yi, A.D. Rao, J. Brouwer, G.S. Samuelsen, Journal of Power Sources 132 (2004) 77–85.
[16] M. Nishiura, S. Koga, T. Kabata, N. Hisatome, K. Kosaka, Y. Ando, Y. Kobayashi, ECS Transactions 7 (2007) 155–160.
[17] C. Stiller, Design, Operation and Control Modelling of SOFC/GT Hybrid Systems, PhD Thesis, NTNU, 2006.
[18] C. Stiller, B. Thorud, O. Bolland, ASME Turbo Expo 2005, 2005.
[19] F. Kroll, A. Nielsen, S. Staudacher, 1st CEAS European Air and Space Conference, 2007.
[20] T. Panne, A. Widenhorn, M. Aigner, ASME Turbo Expo, 2008.
[21] J.B. Hansen, J. Rostrup-Nielsen, Handbook of Fuel Cells, vol. 6, Wiley, Chichester, UK, 2009.
[22] J.M. Sánchez-Hervás, J. Otero, E. Ruiz, Chemical Engineering Science 60 (2005) 2977–2989.
[23] M. Horiuchi, F. Katagiri, J. Yoshiike, S. Suganuma, Y. Tokutake, H. Kronemayer, W.G. Bessler, Journal of Power Sources 189 (2009) 950–957.
[24] W.G. Bessler, S. Gewies, M. Vogler, Electrochimica Acta 53 (2007) 1782–1800.
[25] P. Costamagna, A. Selimovic, M.D. Borghi, G. Agnew, Chemical Engineering Journal 102 (2004) 61–69.
[26] H. Zhu, R.J. Kee, V.M. Janardhanan, O. Deutschmann, D.G. Goodwin, Journal of Electrochemical Society 152 (2005) A2427–A2440.
[27] W.G. Bessler, S. Gewies, C. Willich, G. Schiller, K.A. Friedrich, Fuel Cells 10 (2010) 411–418.
[28] P. Nehter, Journal of Power Sources 164 (2007) 252–259.